# A Numerical Investigation of Breast Compression: Lesion Modeling

**MacArthur L** *mlstewar@oakland.edu Oakland University*
*Stewart/Department of Mechanical Engineering*
*Rochester, MI 48309, USA*

**Lorenzo M. Smith** *L8smith@oakland.edu*
*/ Department of Mechanical Engineering*
*Oakland University*
*Rochester, MI 48309, USA*

**Neal Hall** *NealHall@rossmed.edu*
*Department of Radiology*
*St. Joseph Mercy Hospital*
*Pontiac, MI 48341, USA*

**Abstract**

Researchers have developed finite element (FE) models from preoperative medical images to simulate intraoperative breast compression. Applications for these FE models include mammography, non-rigid image registration, and MRI guided biopsy. Efficient FE breast models have been constructed that model suspect lesions as a single element or node within the FE breast mesh. At the expense of efficiency, other researchers have modeled the actual lesion geometry within the FE breast mesh (conformal breast-lesion mesh). Modeling the actual lesion geometry provides lesion boundary spatial information, which is lost in FE breast models that model suspect lesions as a single element or node within the FE breast mesh.

In this paper, we used a commercial finite element analysis (FEA) program to construct a biomechanical breast model from patient specific MR volumes. A laterally situated lesion was identified in the diagnostic MRI. We used the FE model to simulate breast compression during an MRI guided biopsy. Our objective was to investigate the efficacy of independently discretizing the breast and lesion geometries and using a kinematic constraint to associate the lesion nodes to the nodes in the breast mesh based on their isoparametric position.

This study showed that it is possible to construct an accurate and efficient FE breast model that considers the actual lesion geometry. With 61 mm of breast compression, the lesion centroid was localized to within 3.8 mm of its actual position. As compared to a conformal breast-lesion FE mesh, the element count was also reduced by 53%.

These findings suggest that it is possible to predict the position of a suspect lesion's centroid and boundary within clinical time constraints (< 30 minutes).

**Keywords:** Breast, Finite Element Analysis, Breast Compression, lesions, MRI Guided Biopsy.

## 1. INTRODUCTION

An MRI guided biopsy requires the radiologist to localize the suspect lesion with the breast compressed between rigid plates. However, the suspect lesion is generally identified from a diagnostic MRI exam with breast freely hanging under the force of gravity. There are several potential challenges associated with localizing a suspect breast lesion including patient positioning, visibility of the lesion may fade after contrast injection, menstrual cycles, and lesion deformation. Researchers have constructed FE models that simulate breast compression with the intent of minimizing these challenges [1]. Other applications for these FE breast models included mammography [2], and non-rigid medical image registration [3], [4], [5]. For the researchers selected in this study, three FE lesion modeling methods were considered: 1) the suspect lesion was modeled as an element within the breast mesh, 2) researchers modeled suspect

lesions as point or node within the FE breast mesh, and 3) the actual geometry of the suspect lesion was modeled within the FE breast mesh, conformal breast-lesion mesh.

First, Azar et al. [1] constructed a FE breast model from MRI data of a healthy volunteer using an all hexahedral mesh. The breast contained a cyst, and it was modeled as a single element within the FE breast mesh. These researchers proposed discretizing the breast geometry with an average element size equal to the size of the suspect lesion. The error between the actual and predicted cyst position was (4.4, 1.9, 1.3), in mm.

Second, Zhang et al. [5] constructed a FE breast model from patient specific MRI data using an all tetrahedral mesh, $2^{nd}$ order tetrahedral. A suspect feature was indentified in corresponding mammography images. They modeled the suspect feature by tracking a point in the FE breast model. A suspect lesion was identified in the CC (cranio-caudal) view, and projected to the corresponding compressed FE model. The FE model was decompressed followed by compressing it into the MLO (mediolateral oblique) direction. The predicted position of the suspect lesion was within 2.3 mm of its actual position in the MLO view.

Third, the actual geometry of the suspect lesion was modeled within the solid breast mesh. Maintaining nodal connectivity, the lesion geometry was captured into the breast solid mesh by increasing the mesh density in the vicinity of the lesion and manipulating the position of these nodes to match the lesion's surface profile [3]. This FE modeling method was used to develop a non-rigid image registration validation procedure.

There are pros and cons associated with these lesion modeling methods. Discretizing the breast geometry and differentiating suspect lesions by assigning lesion material properties to elements in the vicinity of the actual lesion is computational efficient; the average element edge length is a function of only the breast geometry's length scale. However, the lesion's length scale is much smaller. The lesion's centroid may be accurately predicted, but the details regarding the boundary of the lesion are lost. In contrast modeling the actual geometry, conformal breast-lesion mesh, eliminates the shortfalls stated above, but it is more computationally expensive. The overall size of the FE breast mesh depends on both the breast and lesion length scales.

The objective of this paper was to investigate the efficacy of independently discretizing the breast and lesion geometries and using a kinematic constraint to associate the lesion nodes to the nodes in the breast mesh based on their isoparametric position. We developed a patient specific biomechanical FE breast model from a diagnostic breast MR volume and the corresponding localizing MR volume from an MRI guided biopsy. The model was used to simulate the associated intraoperative breast compression. The following assumptions were considered in this study:

- Fat and fibroglandular tissues are the primary contributors to the kinematic behavior of the female breast [6]
- Breast tissue is homogeneous, isotropic, nonlinear, and nearly incompressible [7], [8]
- The Neo-Hookean material model adequately models the constitutive relationships of breast tissue [2], [4]
- The breast was allowed to freely hang during the diagnostic MRI
- Prior to compressing the breast in preparation for the biopsy, the breast was allowed to freely hang
- The sternum is stable and reproducible
- The breast coupled with the rigid plates form a conservative system
- For clinical use, predicted results should be available within 30 minutes [1]

Our FEA methodology was verified by visual inspection of the deformed surface profile, calculating the difference between the simulated and actual lesion travel, and overlaying the actual lesion onto the numerical results.

The major contributions to the published literature from this study include:

- Ability to independently discretize the breast geometry and the actual lesion geometry
- Ability to replicate surface boundary conditions including the compression and immobilization plates, and the introducer sheath (biopsy equipment)
- A FE breast model verification method that uses only the breast diagnostic and biopsy MR volumes

## 2. FINITE ELEMENT METHOD AND ELASTICITY FOR MODELING BREAST TISSUE

Constructing a FE model of the female breast requires the analyst to consider nonlinear characteristics. Since the intraoperative breast compression was finite, 61 mm, and the breast tissue material behavior was assumed hyperelastic, nonlinear geometry and nonlinear material theory was considered in this investigation. An overview of nonlinear geometry and nonlinear material theory, applicable to this research, is presented in this section. This section begins with a brief discussion on the linear tetrahedral Herrmann formulated FE element which was used to discretize the computational domain.

### 2.1 GOVERNING FUNCTIONAL

Finite elements that are formulated based on linear elastic theory are not valid for Poisson's ratio (□) approaching 0.5 due to volumetric locking. Volumetric or element locking is a condition that occurs when the element is unable to distort while simultaneously meeting the incompressibility constraint [9]. The numerical solution of these equations may result in large errors due the corresponding kinematic constraints on the admissible displacement fields.

Herrmann formulated finite elements overcome this limitation for incompressible and nearly incompressible materials. In addition to nodal displacement, hydrostatic pressure is an independent variable in the element formulation.

In this research, the FE breast mesh was discretized using the linear tetrahedral Herrmann formulated finite element. This is a 5 node isoparametric element with an additional pressure degree of freedom at each of the four corner nodes [10], Fig. (1). The shape function for the center node is a bubble function. For this reason, the displacements and the coordinates for the element are linearly distributed along the element boundaries. The stiffness of this element is formed using four Gaussian integration points. The degrees of freedom of the center node are condensed out of the element before being assembled in the global matrix [10]. Because of this, it does not add to the computational expense of the FE model.

This element was formulated from the perturbed Lagrangian variational principle,

$$\int_V \left[ W_{dev.} + W_{vol.} - \frac{P^2}{2K} \right] dV - \int_S f_i u_i \, dS, \qquad (1)$$

which is based on the on Herrmann variational theorem [11] [12]. In equation (1), the variables $W_{dev.}$, $W_{vol.}$, P, K, $f_i$, and $u_i$ are the deviatoric strain energy density, volumetric strain energy density, hydrostatic pressure, bulk modulus, nodal load vector, and nodal displacement vector, respectively. Herrmann's variational theorem,

$$\int_V G\left[I_1^2 - 2I_2 + 2\upsilon P I_1 - \upsilon(1-2\upsilon)P^2\right] dV - \int_S f_i u_i \, dS, \qquad (2)$$

and the corresponding differential equation are applicable over the entire range of admissible Poisson's ratios, $0 \le \square \ge 0.5$. The symbols G, $I_1$, and $I_2$ are the shear modulus of elasticity, 1st strain invariant, and 2nd strain invariant, respectively. This functional and the corresponding governing differential equation both describe the same physical problem. The governing differential equation can be derived by considering Euler equations [13], [14]. Equation (2) and its Euler equation counterpart are typically called the weak and strong forms of the governing equation, respectively.

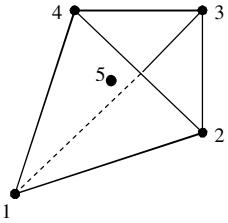


**FIGURE 1:** 1 Linear tetrahedral Herrmann formulated element

### *2.2* Nonlinear Geometry

An MRI guided breast biopsy results in finite breast deformation which means that geometric changes between the undeformed and compressed breast are not negligible. When finite deformations are present, geometric non-linearity should be considered for accurate FE modeling. Geometric non-linearity is usually resolved by writing the equilibrium equations in incremental form [**K**]{□**D**} = {□**R**}. In this mathematical relationship [**K**], {**D**}, and {**R**} are the stiffness matrix, element displacement vector, and nodal load vector, respectively. The [**K**] is a function of {**D**} which is computed iteratively. Iterating continues until the magnitude of the residual force vector is smaller than the specified tolerance. The residual force vector is defined by the difference between the external and internal force vectors. Once the convergence tolerance is satisfied, the current {**D**} becomes the sum of the preceding {□**D**}'s, and the current [**K**] is used to calculate the next displacement increment. The displacement vector and stiffness matrix are updated and the process is repeated until the specified external loading condition is applied. Simply stated, the load-displacement curve is approximated as a series of line segments [13].

In this research, large displacement-large strain theory is assumed. Breast tissue displacements were analyzed in Lagrangian coordinates. The displacement, differentiation, and integration are referenced back to the original domain in the Lagrangian approach. As the displacement increases higher order terms are added to the strain-displacement relationship in order to account for geometric non-linearity. Lagrangian coordinates are typically used where large strains are present [15].

### 2.3 Material Non-linearity

The breast tissue constitutive relationships were modeled using the Neo-Hookean hyperelastic material model. The stress-strain relationship for a hyperelastic material is defined by a strain energy density function,

$$S_i = \frac{\partial W}{\partial \lambda_i}, \tag{3}$$

were $S_i$, W, and $\lambda_i$ are the second Piola-Kirchoff stress, strain energy density, and principle stretches, respectively [15]. Depending on the type of hyperelastic model, the strain energy function is written as a function of strain invariants or stretch ratios, defined in by:

$$\begin{aligned} I_1 &= \lambda_1^2 + \lambda_2^2 + \lambda_3^2 \\ I_2 &= \lambda_1^2 \lambda_2^2 + \lambda_2^2 \lambda_3^2 + \lambda_3^2 \lambda_1^2 \\ I_3 &= \lambda_1^2 \lambda_2^2 \lambda_3^2 . \end{aligned} \tag{4}$$

The terms in equation (4) are derived from the deformation gradient, $F_{ij}$. The deformation gradient maps position vectors in the reference (undeformed) configuration, $X_i$, to the corresponding location in the deformed geometry, $x_i$ [9],

(5)

$$F_{ij} = \frac{\partial x_i}{\partial X_j}; \qquad i, j = 1, 2, 3 .$$

The finite deformation formulation defines the current position of a point, $x_i$, by adding the displacement, $u_i$, to the corresponding reference (undeformed) position of the point, $X_i$ [9],

$$x_i = X_i + u_i . \tag{6}$$

The Neo-Hookean ($W^{NH}$) material model assumes that the strain energy density, elastically stored energy per unit volume, is a polynomial function of the principle strain invariants. This strain energy density function contains only the first order strain invariant term [11],

$$W^{NH} = C_{10}(I_1 - 3). \tag{7}$$

The variable $C_{10}$ is the material parameter which is derived from curve fitting the stress-strain data. Equation (7) is derived by expanding $I_1$, equation (4), into a power series and neglecting higher order terms [15], deviatoric component.

**3.0 MRI Derived Finite Element Breast Model**

Three commercial computer programs were used as our primary research tools. 1) ANALYZE [16] was used to view and manipulate the MR images. ANALYZE is a biomedical image viewing software developed by the Mayo Clinic. 2) The computational domain was discretized using HyperMesh [17]. HyperMesh is a FEA pre-processor, Altair Engineering, Inc. 3) Except for meshing, our FEA model was constructed and processed using MARC/Mentat which is a multi-purpose nonlinear FEA software package, MSC Software Corporation.

Figure 2 gives a general overview on how we constructed our FE model. This section is arranged into 6 subsections that discuss the components of our FE model which include: 1) MRI data and geometry construction, 2) rigid registration, 3) geometry discretization, 4) material properties and material model selection, 5) boundary conditions, and 6) numerical solution methods.

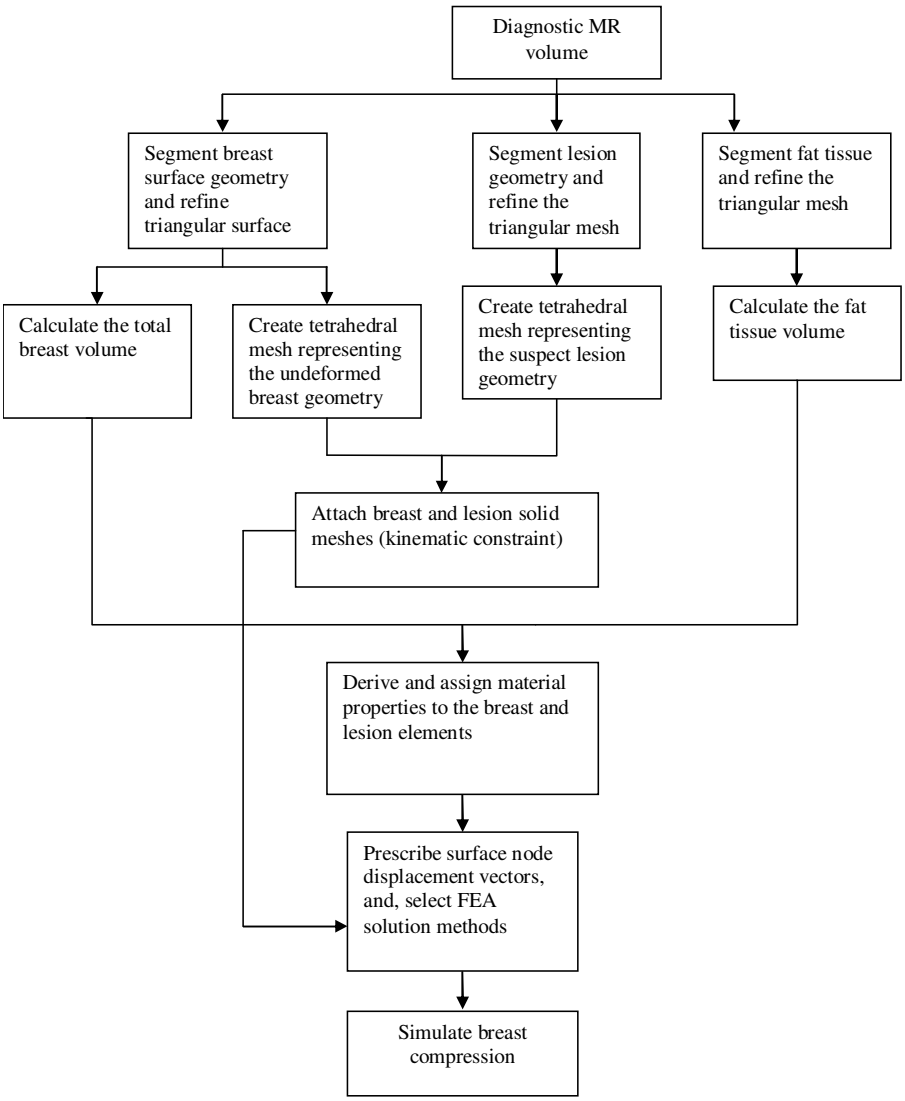


**FIGURE 2:** Overview of the proposed FE breast model construction

### 3.1 MRI Data and Geometry Construction

For this study, the left breast was considered. It contained a single lesion, situated laterally, and was diagnosed as non-invasive cancer. T1-weighted diagnostic and biopsy MR images were acquired. The voxel sizes in the diagnostic and biopsy MR volumes were 0.94x0.94x2.5 $mm^3$ and 0.66x0.66x2 $mm^3$, respectively. The biopsy was performed 18 days after the diagnostic MRI exam**.** Figure 3 contains the 3D rendering of the left breast and a maximum intensity projection (MIP) highlighting the suspect lesion. Figure 4 shows the corresponding biopsy volume.

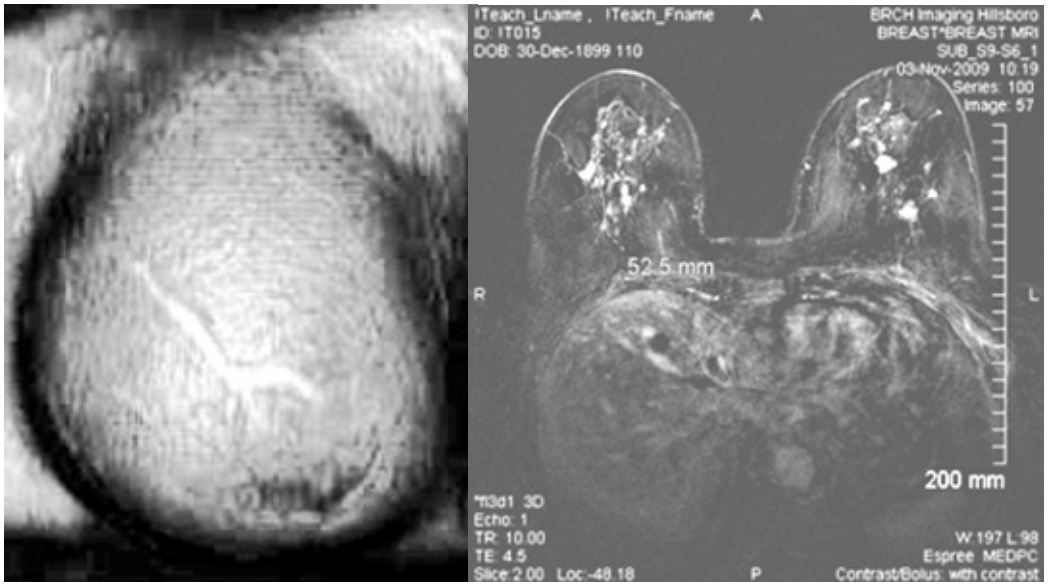


**FIGURE 3:** Breast diagnostic MR volume and a MIP highlighting the suspect lesion

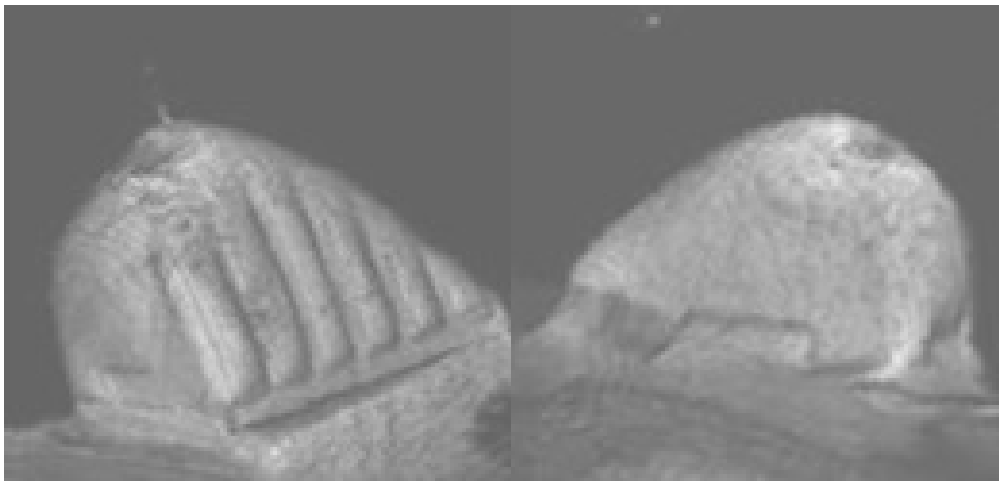

**FIGURE 4:** Breast biopsy MR volume: immobilization plate side (left), compression plate side (right)

### 3.2 MR Volume Rigid Registration

Since the diagnostic and biopsy MR volumes were not aligned, we took an anatomical landmark based registration approach to align these 3D medical images [18]. The sternum was used as the anatomical landmark due to its constant nature [19]. Anatomically, the breast architecture was assumed constant due to scaffolding support by Cooper's ligaments [20]. With sternum alignment, the difference between the two MR volumes was breast compression.

The rigid registration tool in ANALYZE was used to align the two MR volumes, (Fig. 5). This allowed for an independent measurement of lesion displacement (lesion travel from the diagnostic MRI to the biopsy MRI).

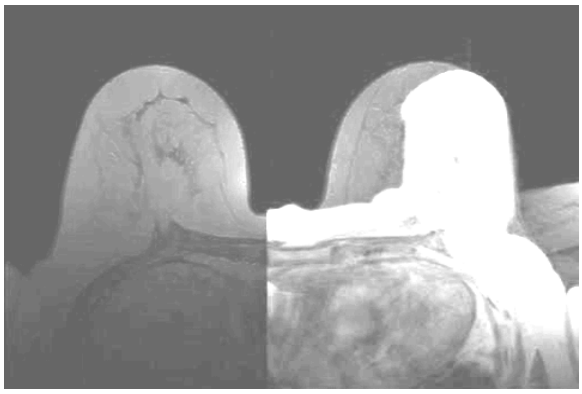

**FIGURE 5:** A 2D MR slice of the biopsy MRI volume (white) overlaid on the diagnostic MR volume (grey), registered at the sternum

### 3.3 Breast and Lesion Geometry Discretization

Figure 6 is a flowchart that describes how the FE breast mesh was constructed; the mesh development process was divided into 5 steps. 1) The diagnostic breast MR images were rendered into a 3D image. 2) Using ANALYZE, we segmented the breast and lesion surfaces from the MR volume. 3) Since the surface mesh quality was insufficient for FEA, these two surfaces were imported into hyperMesh and refined. 4) The breast and lesion surfaces were then independently discretized. The breast surface mesh was discretized resulting in 10,915 tetrahedral elements. The average edge length of the surface elements was 7 mm. The lesion geometry was meshed with a surface element edge length of 0.85 mm resulting in 1,562 tetrahedral elements. 5) We used a kinematic constraint that tied the lesion nodes to the breast nodes based on their isoparametric locations within the breast mesh.

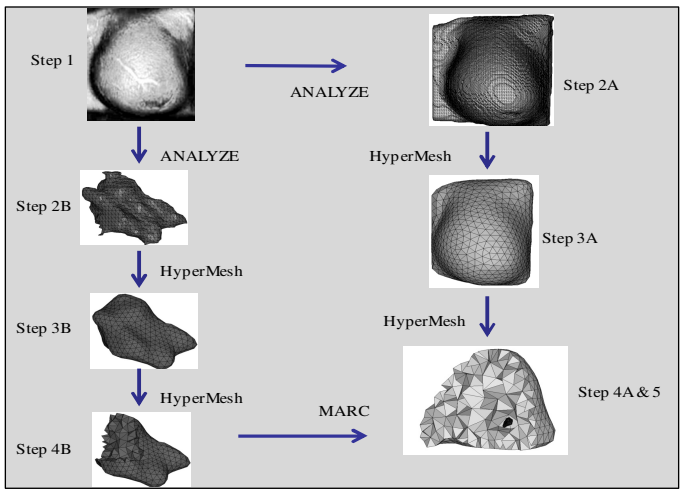


**FIGURE 6:** Breast and lesion geometry discretization process

### 3.4 Elastic Material Properties and Material Model Selection

In this paper, we assumed that the effects of different normal breast tissue types other than the fat and fibroglandular tissues were negligible. In addition, the normal breast tissues were modeled as one tissue type consisting of the volume fractions of the fat and fibroglandular tissues. These volume fractions were calculated by segmenting the fat tissue from the diagnostic MRI and calculating its volume. The total breast volume was also calculated. The fat tissue/total breast volume ratio was 0.67.

Our elastic material properties for the homogeneous breast tissue model were derived by first considering the volume fraction rule,

$$E(\varepsilon)_{breast} = E(\varepsilon)_{fat} V_{fat} + E(\varepsilon)_{fibroglandular}(1 - V_{fat}). \quad (8)$$

The variable $V_{fat}$ is the volume fraction of fat tissue. The functions $E(\square)_{fat}$ and $E(\square)_{fibroglandular}$ were derived by fitting Wellman's [7] experimental derived elastic modulus versus strain data for fat and fibroglandular tissues to third order polynomials. Equation (8) was then integrated with respect to strain ($\square$) resulting in the constitutive relationship for the homogeneous breast tissue model, (Fig. 7).

Using Wellman's [7] material property data for lobular cancer, the constitutive relationship for the suspect lesion was similarly derived. The elastic modulus versus strain data was fitted to a third order polynomial and integrated with respect to strain. The corresponding stress versus strain relationship is also shown in (Fig. 7).

The constitutive relationships for the breast and lesion tissues were imported into Mentat and fitted to the Neo-Hookean material model. $C_{10}$, the Neo-Hookean material parameter, was 1.1 kPa and 4.2 kPa for the breast and lesion tissues, respectively.

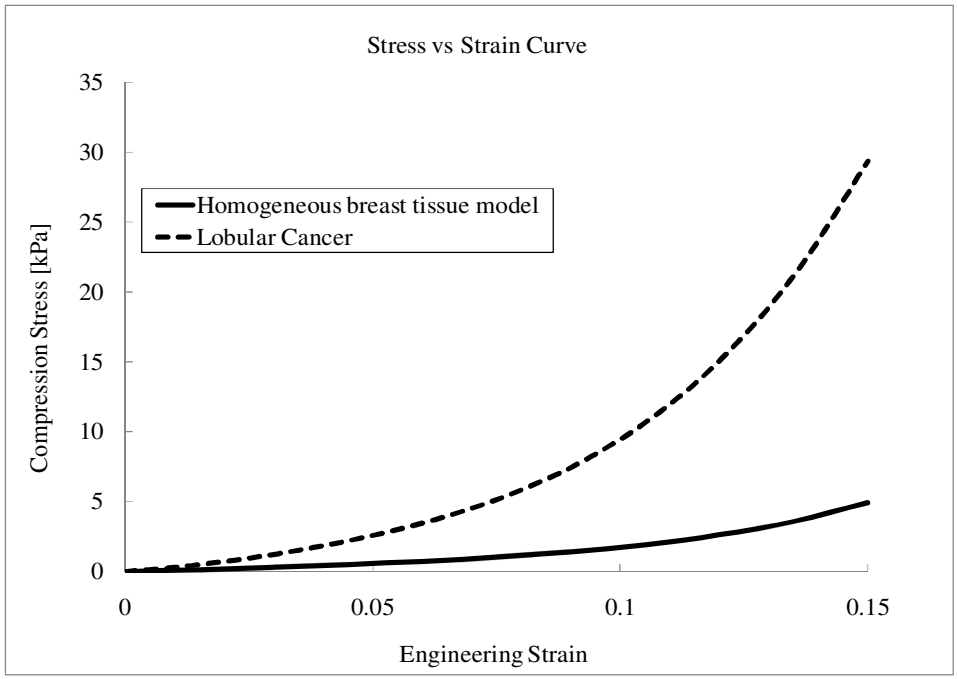


**FIGURE 7:** Homogenous breast tissue model and lesion stress-strain curves

**Boundary conditions**

Fig. 8 is a flowchart that shows how we prescribed a Direchlet boundary condition, displacement vector, to each surface node. The process that we developed to define the nodal displacement vectors contained 5 steps. 1) With the diagnostic and biopsy MR volumes aligned at the sternum, we segmented the breast surface from the biopsy MR volume. Since the mesh quality was inadequate for FE modeling, it was imported into HyperMesh for refinement. 2) The refined surface mesh was then converted into the Initial Graphics Exchange Specification (IGES) surface format using HyperMesh's mesh to geometry surface modification tool. 3) The uncompressed breast surface mesh, which was used to create the FE breast mesh, was morphed onto the deformed breast IGES surface. 4) From the undeformed and morphed breast surface meshes, the displacement vector for each surface node was calculated by subtracting its position vector on the morphed surface mesh from its position vector on the uncompressed surface mesh.

A node versus displacement vector table was created from these calculations. 5) A script was written that converted the node versus displacement table into MARC input deck format. The output from the script was appended to the input deck of the FE breast model.

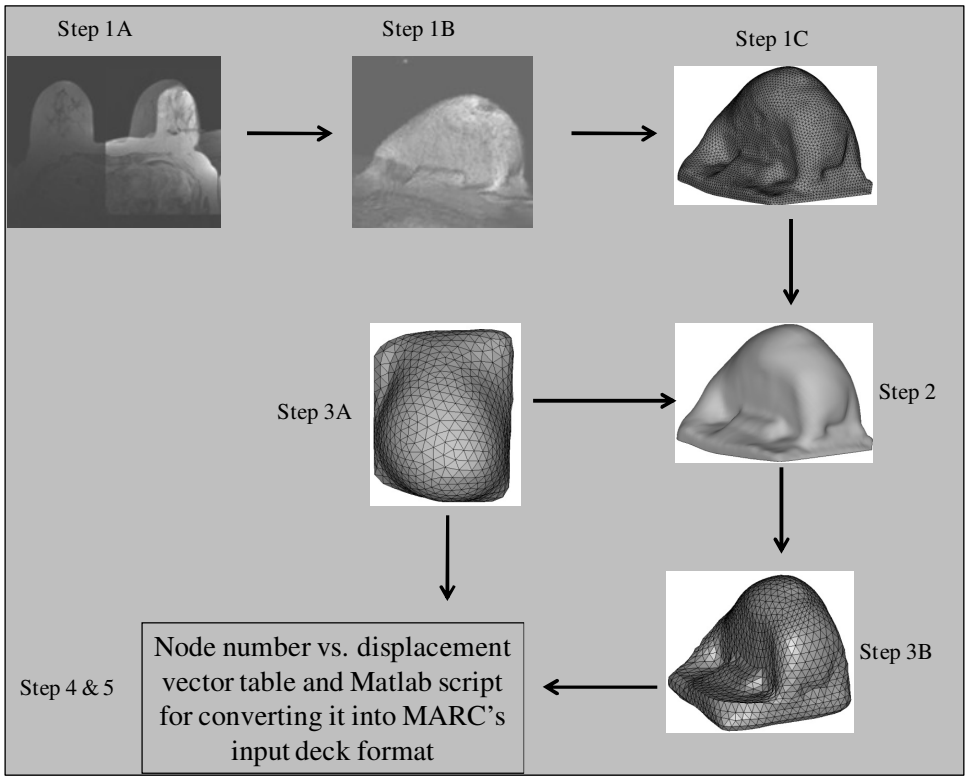


**FIGURE 8:** Construction of surface boundary conditions from the biopsy MR volume

In this study, it was assumed that the nodes at the pectoral fascia and rib interface do not move.

3.6 Finite Analysis Solution

Our FEA methodology for simulating breast compression is summarized here:

- **Element Type**: 12,477 linear tetrahedral, full integration Herrmann formulation
- **Contact**: None
- **Links**: insert kinematic constraint (lesion-breast nodes)
- **Boundary Conditions**: displacement controlled
- **Dynamic Effects**: none (quasi static)
- **Solution Control**: large displacement, large strain, Lagrangian, Newton-Raphson
- **Stepping Procedure**: Constant time step
- **Convergence Criteria**: Relative residual force magnitude, criteria ≤ 0.1

**4.0 RESULTS**

We constructed 3 additional FE models that differ only in how the suspect lesion was modeled. 1) The lesion was modeled as a rectangular prism made up of 77 tetrahedrals. The suspect lesion was bound by the rectangular prism, similar to the work of Azar et al. [1] 2) A single node representing the centroid of the suspect lesion within the FE breast mesh. Zhang et al. [5] used this method to track a suspect breast feature that was identified on mammographic images. The normal and lesion breast tissue were modeled

as one tissue type consisting of the volume fractions of the fat and fibroglandular tissues. 3) The actual lesion geometry was modeled within the FE breast mesh; a conformal breast-lesion mesh; this method was proposed by Schnabel et al. [3]. The results of these models were compared to the proposed FE model.

The results are arranged into 3 subsections: 1) Deformation contour plots, 2) suspect lesion travel, and 3) suspect lesion overlaid onto the FEA results.

### 4.1 Deformation Contours Plots

As expected, the displacement contour plots for the four FE lesion models were similar. Figure 9 shows the common displacement contour plot overlaid on the deformed FE breast model after the surface boundary conditions were applied. The deformed surface profile replicates the surface profile of the biopsy MR volume. The peak compression and immobilization plate travel was 46 mm and 15 mm, respectively.

In comparison to the conformal breast-lesion FE mesh, the element count for the proposed FE breast mesh was reduced by 53%, from 26,299 to 12,4777 elements. The corresponding time required to apply the surface boundary conditions was reduced from 42 minutes to 3 minutes. The FE model size and processing time differences between models 1, 2, and the proposed FE breast model were negligible.

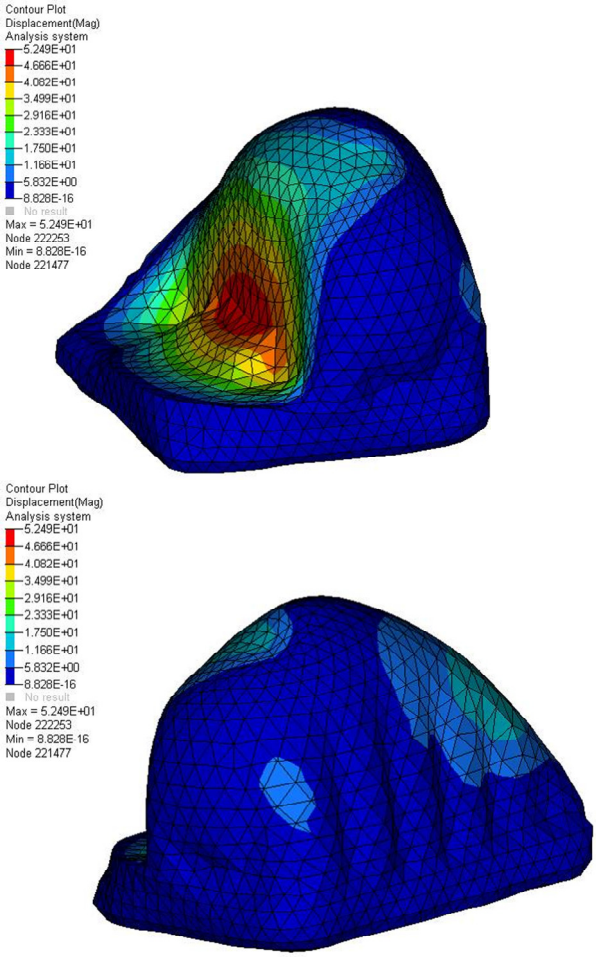


**FIGURE 9:** Displacement contour plots: view from the compression plate side (top) view from the immobilization plate side (bottom)

### 4.2 Suspect Lesion Travel

ANALYZE was used to calculate the position coordinates of the suspect lesion's centroid in the undeformed and compressed breast volumes. The lesion's displacement vector was calculated by subtracting the lesion's position vector in the biopsy MR volume from the lesion's position vector in the diagnostic MR volume. The centroidal coordinates, in mm, of the lesion from the diagnostic and biopsy MR volumes were (79.7, 219.3, 44.5) and (68.7, 218, 40.1), respectively. From this, the lesion displacement vector was (11, 1.3, 4.3); the corresponding magnitude was 11.9 mm.

Table 1 shows the lesion displacement error from each of the 4 methods used to model the suspect lesion. With 61 mm of breast compression, the proposed FE breast model localized the suspect lesion to within 3.8 mm of its actual position. The accuracy limit for adequate registration is 5 mm [2]. As compared to previously published lesion modeling techniques, the simulation results from the proposed method were provides similar accuracy. Thus, our method for modeling breast lesions may offer the combined benefits of previous researchers without the inherent limitations.

**TABLE 1:** Lesion Centroid Position Error (mm)

| | Lesion FE Model | X | Y | Z | Lesion Centroid Position Error |
|---|---|---|---|---|---|
| 1 | Specific Elements within the FE breast Mesh | 2.7 | 1.1 | 2.3 | 3.7 |
| 2 | Single node representing the lesion's centroid within the FE breast Mesh | 2.7 | 1.1 | 2.4 | 3.8 |
| 3 | Actual Lesion geometry within the FE breast Mesh (Confromal breast-lesion mesh) | 2.2 | 1.5 | 2.3 | 3.5 |
| 4 | Actual Lesion geometry within the FE breast Mesh (kinematic constraint) | 2.8 | 1.2 | 2.3 | 3.8 |

### 4.3 Suspect Lesion Overlaid Onto the FEA Results

Figure 10 shows the actual lesion (right) segmented from the biopsy MR volume, overlaid onto the FEA results (left) from the proposed FE model. The surface areas of the lesion segmented from the diagnostic and biopsy MRI's were 310 $mm^2$ and 353 $mm^2$, respectively. The overlapping surface area was 165 $mm^2$. Using the lesion surface area from the diagnostic MR volume, this resulted in 45% overlap. CAD tools were used to calculate the lesion surface areas. The overlapping surface area was created from the intersection of the lesion surfaces.

It is hypothesized that the deviation between these surfaces was due, primarily, to the anisotropic nature of breast tissue [21] and the difference in lesion visualization between the diagnostic and biopsy MR volumes. Breast tissue anisotropy is beyond the scope this paper; modeling anisotropic material behavior may increase the amount of overlap between the actual and predicted lesion positions and should be considered in future research.

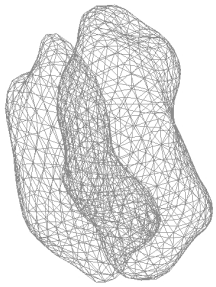

**FIGURE 10:** The actual lesion (left) overlaid onto the FEA results (right). The amount of overlap is highlighted (black)

## 5. 0 DISCUSSION

Potentially, radiologists would use our method for modeling suspect lesions, in combination with FEA methods developed by previous researchers, to assist in targeting suspect lesions that are difficult to localize with the breast compressed between rigid plates. Previous researchers have developed stand alone algorithms for segmenting and discretizing the breast surface, lesions, and the fibroglandular tissue region. The physician would simulate breast compression in 3 stages: 1) with the sternum used as a rigid registration feature, they would align the diagnostic and biopsy MR volumes, 2) patient specific suspect lesions would be independently discretized based on their own length scales, and 3) with the lesion meshes kinematically constrained to the corresponding breast mesh, the patient specific FE breast model would then be used to predict the position of the suspect lesion (centroid and boundary positions).

## 6.0 CONCLUSION

In conclusion, this research made three points. 1) The breast and lesion geometries can be independently discretized. A kinematic constraint that tied the lesion nodes to the corresponding nodes in the breast mesh based on their isoparametric position was an enabler for independent breast and lesion meshing. 2) Constructing the surface from the biopsy MR volume and using it to define displacement vectors for the surface of the breast mesh is a viable alternative to prescribing boundary conditions. With this method, the effects of external contacting bodies are considered without having to directly model them. 3) As compared to the conformal breast-lesion mesh, the FE model sized was reduced by 53%.

Since our FEA method was demonstrated on a single case, our evidence is limited to this patient. For this reason, we will use our proposed FEA method to study additional cases. These additional cases will include different types of suspect lesion tissue, lesions situated in different quadrants of the breast, and multiple suspect lesions (dual biopsy).

## 7.0 ACKNOWLEGEMENTS

The authors would like to thank Dr. Kathy Schilling, Medical Director of Imaging and Intervention for the Boca Radiology Group in Boca Raton, FL. Dr. Schilling supplied the MR image volumes and the corresponding diagnostic detail.

## REFERENCES

[1] F.S. Azar, D.N. Metaxas, M.D. Schnall. "Methods for modeling and predicting mechanical deformations of the breast under external perturbations". IEEE Workshop on Mathematical Methods in Biomedical Image Analysis, 6(1):1-27, 2002

[2] N.V. Ruiter, R. Stotzka, T.O. Muller, H. Gemmeke. "Model-based registration of X-ray mammograms and MR images of the female breast". IEEE Symposium Conference on Nuclear Science, 5:3290- 3294, 2004

[3] A. Schnabel, C. Tanner, A.D. Castellano-Smith, A. Degenhard, M.O. Leach, D.R. Hose, D.L.G. Hill, D.J. Hawkes. "Validation of Nonrigid Image Registration Using Finite-Element Methods: Application to Breast MR Images". IEEE Transactions on Medical Imaging, 22(2):238-247, 2003

[4] A. Samani, A.J. Bishop, M.J. Yaffe, D.B. Plewes, 2001. "Biomechanical 3-D Finite Element Modeling of the Human Breast Using MRI Data". IEEE Trans. Medical Imag., 20(4):271-279, 2001

[5] O. Zhang, A. Qiu, D.B. Goldgof, S. Sarkar, L. Li. "3D Finite Element Modeling of Nonrigid Breast Deformation for Feature Registration in X-ray and MR Images". IEEE Workshops on Applications of Computer Vision, :38-44, 2007

[6] A. Perez del Palomar, B. Calvo, J. Herrero, J. Lopez, M. Doblare. "A Finite Element Model to Accurately Predict Real Deformations of the Breast". Medical Engineering & Physics, 30(9):1089-1097, 2008

[7] P.S Wellman. "Tactile Sensing". PhD. Thesis, Harvard University, 1999

[8] T.A Krouskop, T.M. Wheeler, F. Kallel, B.S. Garra, T. Hall. "Elastic Moduli of Breast and Prostate Tissues Under Compression". Ultrasonic Imaging, 20: 260-274, 1998

[9] J. Bonet, R. Wood. R. "Nonlinear Continuum Mechanics for Finite Element Analysis", Cambridge University Press, pp. 57-64. (1997)

[10] MSC Software Corporation. "Volume B: Element Library", 2005

[11] MSC Software Corporation. "Volume A: Theory and User Manual", 2005

[12] L.R. Herrmann, R.M. Toms. "A reformulation of the Elastic Field Equations in Terms of Displacements, Valid for All Admissible Values of Poisson's Ratio". Journal of Applied Mechanics 31: 148-149, 1964

[13] R.D. Cook. "Concepts And Applications of Finite Element Analysis 2nd Edition, John Wiley & Sons, pp. 351-353, 1981

[14] L.R. Herrmann. "Elasticity Equations for Incompressible and Nearly Incompressible Materials by a Variational Theorem". American Institute of Aeronautics and Astronautics (AIAA) 10:1896-1900, 1965

[15] A.N. Gent. "Engineering with Rubber: How to Design Rubber Components", Hanser Gardner Publications, pp. 50-54, 2001

[16] AnalyzeDirect. "Analyze 10.0 Essential Training Guide", 2010

[17] Altair Engineering. "HyperMesh 10.0, User Manual", 2010

[18] I.N. Bankman. "Handbook of Medical Imaging Processing and Analysis", Academic Press, pp. 499-500, 2000

[19] M. Betke, H. Hong, D. Thomas, C. Prince, J. Ko. "Landmark Detection in the Chest and Registration of Lung Surfaces with an Application to Nodule Registration". Journal of Medical Image Analysis: 265-281, 2003

[20] F.H. Netter. "Atlas of Human Anatomy, 2nd ed", Navortis, pp. 167-169, 1997

[21] C. Tanner, M. White, S. Guarino, S, M.A. Hall-Craggs, M. Douek, M. D.J. Hawkes. "Anisotropic Behavior of Breast Tissue for Large Compressions". IEEE International Symposium on Biomedical Imaging: From Nano to Macro:1223-1226, 2009